AGU PUBLICATIONS

Water Resources Research

RESEARCH ARTICLE

10.1002/2013WR014753

Snowpack regimes of the Western United States

Ernesto Trujillo[1,2] and Noah P. Molotch[2,3,4]

[1]Laboratory of Cryospheric Sciences, School of Architecture, Civil and Environmental Engineering, École Polytechnique Fédérale de Lausanne, Lausanne, Switzerland, [2]Institute of Arctic and Alpine Research, University of Colorado, Boulder, Colorado, USA, [3]Department of Geography, University of Colorado, Boulder, Colorado, USA, [4]Jet Propulsion Laboratory, California Institute of Technology, Pasadena, California, USA

Key Points:
- No proportionality in the SWE curve is inferred in the Western United States
- Relationships between SWE metrics highlight the natural snowpack patterns
- SWE metrics offer basis for comparison of current and future snowpack dynamics

Supporting Information:
- List and captions of supplementary figures
- Supplementary figure S1
- Supplementary figure S2
- Supplementary figure S3
- Supplementary figure S4
- Supplementary figure S5
- Supplementary figure S6
- Supplementary figure S7
- Supplementary figure S8
- Supplementary figure S9
- Supplementary figure S10

Correspondence to:
E. Trujillo,
Ernesto.Trujillo@epfl.ch

Citation:
Trujillo, E., and N. P. Molotch (2014), Snowpack regimes of the Western United States, *Water Resour. Res.*, *50*, doi:10.1002/2013WR014753.

Received 19 SEP 2013
Accepted 8 JUN 2014
Accepted article online 11 JUN 2014

Abstract Snow accumulation and melt patterns play a significant role in the water, energy, carbon, and nutrient cycles in the montane environments of the Western United States. Recent studies have illustrated that changes in the snow/rainfall apportionments and snow accumulation and melt patterns may occur as a consequence of changes in climate in the region. In order to understand how these changes may affect the snow regimes of the region, the current characteristics of the snow accumulation and melt patterns must be identified. Here we characterize the snow water equivalent (SWE) curve formed by the daily SWE values at 766 snow pillow stations in the Western United States, focusing on several metrics of the yearly SWE curves and the relationships between the different metrics. The metrics are the initial snow accumulation and snow disappearance dates, the peak snow accumulation and date of peak, the length of the snow accumulation season, the length of the snowmelt season, and the snow accumulation and snowmelt slopes. Three snow regimes emerge from these results: a maritime, an intermountain, and a continental regime. The maritime regime is characterized by higher maximum snow accumulations reaching 300 cm and shorter accumulation periods of less than 220 days. Conversely, the continental regime is characterized by lower maximum accumulations below 200 cm and longer accumulation periods reaching over 260 days. The intermountain regime lies in between. The regions that show the characteristics of the maritime regime include the Cascade Mountains, the Klamath Mountains, and the Sierra Nevada Mountains. The intermountain regime includes the Eastern Cascades slopes and foothills, the Blue Mountains, Northern and Central basins and ranges, the Columbia Mountains/Northern Rockies, the Idaho Batholith, and the Canadian Rockies. Lastly, the continental regime includes the Middle and Southern Rockies, and the Wasatch and Uinta Mountains. The implications of snow regime classification are discussed in the context of possible changes in accumulation and melt patterns associated with regional warming.

1. Introduction

Climatic conditions vary significantly from maritime to continental climates with strong gradients in precipitation, temperature, and seasonality. These differences strongly influence snow accumulation and snowmelt patterns in the Western United States and other mountainous regions globally. For example, winter precipitation in coastal regions of the Western U.S. is strongly influenced by atmospheric rivers (AR's), with differences in frequency of winter AR's from north to south [*Neiman et al.*, 2008; *Guan et al.*, 2010]. On the other hand, winter precipitation patterns in the continental regions are generally influenced by the El Nino Southern Oscillation [*McCabe and Dettinger*, 1999] and by land-atmosphere interactions [*Rasmussen et al.*, 2011]. Such differences lead to marked variability in snow accumulation between maritime and continental regions. Similarly, winter and spring air temperatures are warmer in maritime versus continental climates leading to differences in snowpack microstructure [*Sturm et al.*, 1995], snowpack cold content, and the timing and magnitude of snowmelt [*Gray and Male*, 1981]. Characterizing these differences is important for understanding socioecological response to changes in climate.

Identification of snowpack dynamics within climatic regimes is important for determining how changes in climate and land cover influence snow accumulation and snowmelt, as various perturbations and forcings may result in the crossing of thresholds whereby system behavior is significantly and indefinitely altered. As a top-down driver of hydrologic response to climate and land use change in mountainous regions, changes in snowmelt dynamics are difficult to diagnose absent a unifying framework to establish current regime behavior and therefore determine if snowpack conditions have changed in some manner. Drivers inducing

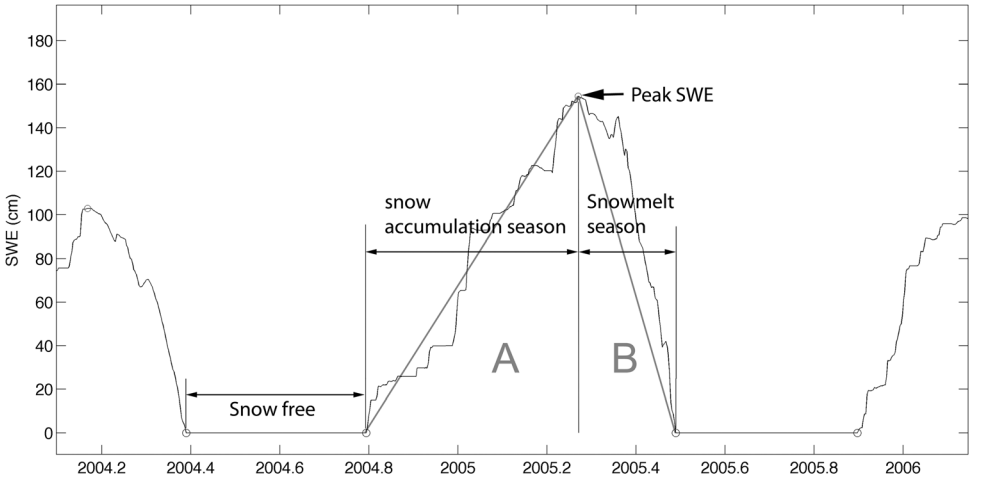

Figure 1. Daily snow water equivalent curve for an accumulation and melt season displaying a sketch of the basic metrics that can be used to characterize snowpack dynamics at a particular station. Metrics (1), (2), and (3) mark the day of initial snow accumulation, peak SWE, and snow disappearance, respectively. Metric (4) marks the peak SWE value. A and B indicate the accumulation and melt seasons, respectively.

these changes include changes in snow surface albedo associated with changes in impurity concentrations [*Painter et al*., 2010], changes in temperature associated with regional warming [*Stocker et al*., 2013], changes in interception and surface-atmosphere energy exchange associated with fire [*Harpold et al*., 2013], and insect and climate-related forest mortality [*van Mantgem et al*., 2009; *Pugh and Gordon*, 2012]. Snowmelt response to these perturbations in turn impacts regional climate via the snow-albedo feedback [*Hall and Qu*, 2006; *Flanner et al*., 2011] and via changes to sensible and latent heat fluxes associated with snowmelt controls on soil moisture [*Molotch et al*., 2009]. Identification of snow regimes also provides a framework for cross-site comparisons [*Marks and Winstral*, 2001], observation network design [*Molotch and Bales*, 2005], and model comparison studies [*Rutter et al*., 2009]—all of which have general hydrologic applicability [*Wagener et al*., 2007].

Comparative studies from different environments are common in the literature [e.g., *Molotch et al*., 2009; *Rutter et al*., 2009; *Tague and Dugger*, 2010] but similar to the catchment hydrology community, lacking is a unifying classification framework to facilitate meaningful and efficient cross comparisons [*Wagener et al*., 2007]. Identification of snow regimes is therefore critical for establishing a baseline for these comparative studies.

The basis for identifying snow regimes relates to the prevailing precipitation, temperature, and other climatic parameters from site to site. Within the Western U.S., these climatic variables change from maritime to continental climates, yet the nature at which these climatic differences reveal themselves in the snow observational record has been limited to analyses of precipitation and SWE [*Serreze et al*., 1999, 2001; *Knowles et al*., 2006]. In particular, a detailed accounting as to how differences in climate across the region influence the shape of the snow water equivalent curve (i.e., the time series of SWE across the snow season including accumulation and ablation) has been lacking.

A time series plot of continuously measured SWE (hereafter referred to as the SWE curve) often takes on a shape in which certain proportions of the curve are generally maintained from year to year, and in some cases, from place to place. For example, a relatively shallow accumulation slope occurs until a maximum SWE value is reached, followed by a steeper decrease in SWE indicating higher snowmelt versus accumulation rates (e.g., Figure 1). Such representation can be compared to that of a river hydrograph following a precipitation event, for which a simplified representation was proposed by *Rodríguez-Iturbe et al*. [1979]. Their representation uses a set of metrics to represent a triangular shape in which the commencement of the rising limb, peak streamflow, and the end point of the falling limb of the hydrograph are represented. Similarly, a simplified representation can be explored for the SWE curve. The overarching objectives of this study are to determine if there is any proportionality in the snow water equivalent curve on the basis of hydrologically relevant metrics of the SWE curve, and if different regions exhibit differences in the

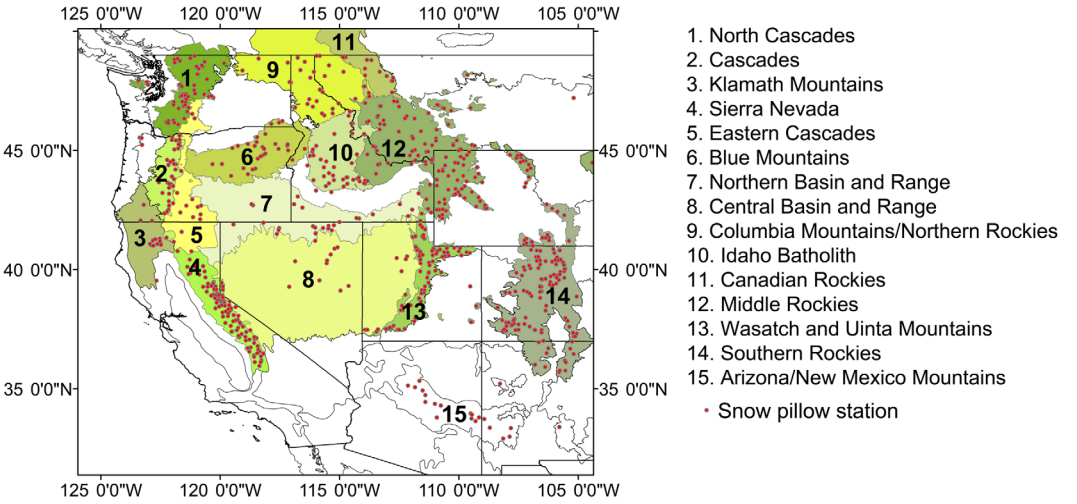

Figure 2. Location of snow pillow stations and study regions delineated using the Commission for Environmental Cooperation (CEC) Ecological Regions of North America, Level III [*Commission for Environmental Cooperation*, 2009, available at http://www.epa.gov/wed/pages/ecoregions/na_eco.htm].

characteristics of the SWE curve on the basis of these metrics. These objectives are addressed through the analyses of (a) the proportionality of the SWE curve based on the interrelationships between the length of the accumulation and snowmelt seasons, peak SWE, and snow season duration, all of which fully characterize the triangle in Figure 1, (b) the interrelationships between the dates of initial accumulation, peak SWE and disappearance, maximum accumulation, and ablation slope, (c) regional differences in accumulation dynamics, and (d) regional differences in ablation dynamics.

2. Methods and Data

The data set used compiles the daily time series of SWE measured at Snowpack Telemetry (SNOTEL) snow pillow stations managed by the United States Natural Resources Conservation Service (NRCS), and SWE observations from snow pillow stations managed by the California Department of Water Resources. The analyses focus on a set of metrics of the SWE curve to characterize the important characteristics of the time series. In this regard, we simplify the SWE curve as a triangular shape in which the vertices of the triangle represent metrics that are of particular relevance for hydrologic purposes (Figure 1). The first four metrics define the vertices of the triangle: (1) the day of water year (DOWY) of initial snow accumulation; (2) DOWY of peak SWE; (3) DOWY of snow disappearance; and (4) peak annual SWE. Metrics 5–7 are then derived from the triangle: (5) the length of the snow accumulation season—i.e., the difference between (1) and (2) above; (6) the length of the snowmelt season—i.e., the difference between (2) and (3) above; and (7) the ablation slope, obtained by dividing the peak SWE value (metric 4) by the length of the snowmelt season (metric 6).

All snow pillow stations in the Western U.S. were initially compiled, processed, and visually inspected to evaluate the quality of the record. The resulting data set includes 766 stations, with period of record between 1964 and 2009, with a sharp increase in available stations starting in the early 1980s. The resulting data set includes 18,759 station-years. The stations were organized in subgroups using the boundaries of the Commission for Environmental Cooperation (CEC) Ecological Regions of North America, Level III [*Commission for Environmental Cooperation*, 2009, available at http://www.epa.gov/wed/pages/ecoregions/na_eco.htm] (Figure 2). These boundaries were delineated in a holistic and comprehensive manner according to seven categories that include location, climate, vegetation, hydrology, terrain, wildlife, and land use, separating regions with the amount of detail desired for our analysis. These ecoregion boundaries were used with a slight modification of the boundary of the North Cascades ecoregion, for which the area and stations located north of the Columbia River originally within the Cascades ecoregion were reclassified as part of the Northern Cascades to increase the sample size for this region and to split the available information more uniformly across the Pacific Northwest.

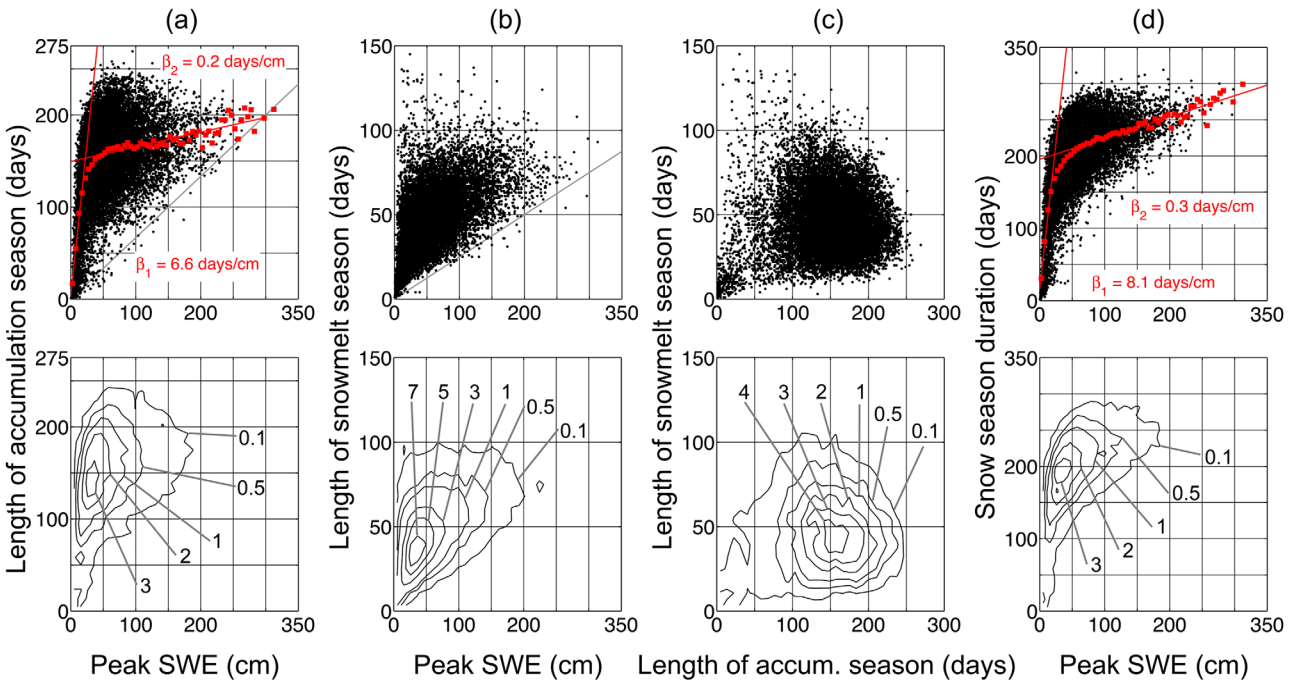

Figure 3. Proportions of the snow water equivalent curve from the snow pillow stations in the Western U.S. The scatter plots (top) include (a) 16,478 year-pairs, (b) 16,633 year-pairs, and (c, d) 16,404 year-pairs. The contour plots (bottom) show the density of points in the scatter plots (i.e., points per unit area: #-points/cm/d in Figures 3a, 3b, and 3d, and #-points/d^2 in Figure 3c). The gray diagonal lines in the (a, b) scatter plots mark an accumulation slope of 1.5 cm/d and an ablation slope of 4 cm/d, respectively, and are included as a reference to mark accumulation and ablations slopes below which the majority (>99.5%) of the year-pairs are located.

3. Results

3.1. Proportionality of the Snow Water Equivalent Curve

We characterize the proportionality of the SWE curve by looking at the relationships between the length of the snow accumulation season (metric 5) versus peak SWE (metric 4) (Figure 3a), length of the snowmelt season (metric 6) versus peak SWE (metric 4) (Figure 3b), length of the snowmelt season (metric 6) versus length of the snow accumulation season (metric 5) (Figure 3c), and the total snow season duration (i.e., the sum of metrics 5 and 6) versus peak SWE (metric 4) (Figure 3d). These relationships are equivalent to analyzing the proportions of a triangle separated in two as in Figure 1, with the portion "A" representing the accumulation season and portion "B" representing the melting season.

From a generalized perspective, there are certain proportions that are more frequent (see contour lines in Figure 3 (bottom)), although significant scatter is observed around such proportions. These more frequent proportions are (a) a snow accumulation season length of around 150 days versus a peak SWE value of about 35 cm (Figure 3a), (b) a snowmelt season length of about 40 days versus a peak SWE value of 35 cm (Figure 3b), (c) a snow accumulation season length of 150 days versus a snowmelt season length of 40 days (Figure 3c), and (d) a snow cover duration of about 190 days versus a peak SWE value of 35 cm (Figure 3d). Average accumulation and melt rates are in the large majority (99.5% and 99.9% of cases) below 1.5 and 4.0 cm/d, respectively (i.e., gray lines in Figures 3a and 3b).

Mean accumulation season length as a function of peak SWE (red squares in Figure 3a with linear regression slopes β_1 and β_2 for the lower and higher peak SWE values, respectively) show a steep increase in accumulation season lengths following a slope of 6.6 d/cm below 23 cm of SWE (intersect between the β_1 and β_2 slopes), and a much milder slope of 0.2 d/cm for the higher peak SWE values. The intersect of the two slopes will be used hereafter as a quantitative measure of the change in the relationships between metrics where appropriate, following the nomenclature of β_1 and β_1 as the slopes of the regression lines in the lower and higher range of the metric in the *x* axis. Also, years with the largest snow accumulations do not correspond with the longest accumulation seasons or the longest ablation seasons. The longest accumulation seasons are found for peak SWE values between 50 and 150 cm SWE, while the longest snowmelt

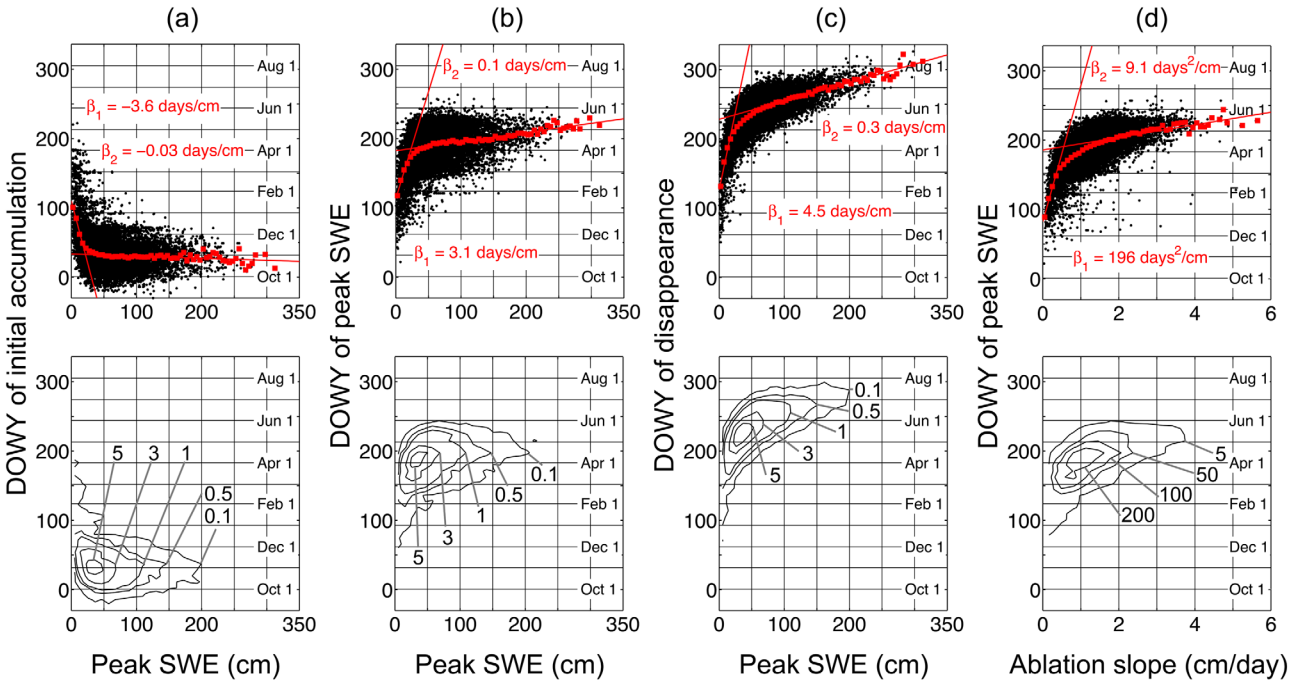

Figure 4. Relationships between the maximum accumulations and ablation slopes and metrics of the timing of the snow cover over the Western U.S. The scatter plots (top) include (a) 16,478 year-pairs, (b) 16,727 year-pairs, and (c, d) 16,633 year-pairs. The contour plots (bottom) show the density of points in the scatter plots (i.e., points per unit area: #-points/cm in Figures 4a–4c, and #-points/cm in Figure 4d).

seasons are seen for peak SWE values lower than 150 cm (Figures 3a and 3b). Regarding the duration of the accumulation and melt seasons, the length of the accumulation season is longer than the corresponding snowmelt season in the majority of cases (Figure 3c). Lastly, there is a general increasing trend in the snow season duration with peak SWE. Mean snow season duration as a function of peak SWE (red squares in Figure 3d) show a steep increase following a slope of 8.1 d/cm below 23 cm of Peak SWE, above which the slope converges to a much milder rate of 0.3 d/cm.

3.2. Relationships Between the Timing and Magnitude of Snow Accumulation and Snowmelt

Similar to the proportionality analysis above, we look at the relationships between the metrics associated with the timing (DOWY) of initial accumulation, peak accumulation, and snow disappearance versus peak accumulation and ablation slope. With these comparisons, we show the relationships between temporal metrics of the SWE curve and the two most hydrologically relevant metrics, i.e., peak snow accumulation and average snowmelt rate. These comparisons include the DOWY of initial accumulation versus peak SWE (Figure 4a), DOWY of peak SWE versus peak SWE (Figure 4b), DOWY of disappearance versus peak SWE (Figure 4c), and DOWY of peak SWE versus the ablation slope (Figure 4d).

Mean dates of initial accumulation decrease with Peak SWE following a linear slope (β_1) of −3.6 d/cm below 22 cm of SWE (intersect), above which the date of initial accumulation decreases at a rate of only −0.03 d/cm (β_2), indicating little change in the mean dates of initial accumulation for the deeper snowpacks (Figure 4a). Similar relationships but opposite in sign are observed for both the mean dates of peak SWE and disappearance as a function of peak SWE (Figures 4b and 4c). Mean dates of peak accumulation increase rapidly with peak SWE following a slope of 3.1 d/cm (β_1) for shallower snowpacks (<23 cm SWE based on the intersect of the regression lines with slopes β_1 and β_2), above which the relationship converges to a slope of 0.1 d/cm, again illustrating a weak relationship between dates of maximum accumulation and peak SWE for deeper snowpacks. Similarly, dates of disappearance increase with peak SWE following a steep slope of 4.5 d/cm below 23 cm SWE (intersect), converging gradually to a slope of 0.3 d/cm at about 50 cm SWE. Lastly, mean dates of maximum accumulation displays a similar relationship with ablation slope, with a rapid

increase following a slope of 196 d^2/cm below 0.55 cm/d (intersect), above which the relationship converges gradually to a slope of 9.1 d^2/cm above an ablation slope of 1 cm/d (Figure 4d).

Regarding the variability of around the average behavior, initial accumulation, peak accumulation, and snow disappearance occur over a wide range of dates between early October to June for shallower snowpacks ($<$23 cm SWE; Figures 4a–4c). These shallower snowpacks also have shorter snow accumulation and snowmelt seasons and in consequence, short snow cover duration. These snowpacks are generally located at lower elevations and/or in regions with discontinuous snow cover that undergo several accumulation and melt cycles during the winter months (e.g., Arizona/New Mexico). Such accumulation and melt cycles lead to wide ranges in the timing of the main SWE curve; example SWE curves are shown in Figure S1 (see supporting information). Note that the metrics in this analysis are obtained for the main SWE curve; i.e., the curve for which the peak annual SWE occurs. However, for station-years with intermittent snow cover, there may be several snow accumulation and melt cycles prior to and/or after the main SWE curve which are not accounted for in this analysis. Deeper snowpacks (Peak SWE $>$ 23 cm) start accumulating between mid-September and mid-December, with only a few examples accumulating between mid-December and February toward the lower end of the peak SWE range between 23 and 50 cm. The deepest snowpacks (peak SWE $>$ 150 cm) start accumulating during a narrower range between the beginning of October and the end of November (Figure 4a). Similarly, for these deeper snowpacks, the peak is reached over a wide range of dates between mid-February and the end of May. The scatter plot also shows that the deepest snowpacks can last until early to mid-August. Lastly, snowpacks that reach peak values later in the year melt faster, as indicated by the higher ablation slopes in Figure 4d. This observation is particularly important for hydrologic, ecological, and geomorphological purposes, as higher melt rates indicate a faster release of meltwater with implications for flood risk, groundwater recharge, mineral weathering, plant water availability, and nutrient cycling.

3.3. Regional Differences in Accumulation Dynamics

Here we focus on the length of the accumulation season, and the peak SWE values to represent water storage in the snowpack. When the year-pairs within each of the ecoregions are highlighted within the point-cloud in Figure 5, three subgroups/regimes emerge which correspond remarkably well with the climatic regimes in the Western U.S.: a maritime, an intermountain, and a continental regime. The ecoregions in the maritime regime exhibit the largest snow accumulations, reaching values as high as over 300 cm of SWE, and the shortest snow accumulation season lengths with the majority of values below 220 days (e.g., the Northern Cascades and Sierra Nevada Mountains in Figures 5a and 5b, respectively). As a result, the maritime point-cloud occupies the lower-right portion of the comprehensive point-cloud. The distribution of the points can be better observed in the inset boxes located in the lower-right quadrant of the plots in Figures 5a and 5b, with the mean length of the accumulation season following a steep linear increase with peak SWE for the shallower snowpacks ($\beta_1 = 5.1$ and 3.0 d/cm in Figures 5a and 5b, respectively), while a milder slope for the deeper snowpacks ($\beta_2 = 0.27$ and 0.29 d/cm in Figures 5a and 5b, respectively). The intersect of these regression lines is located at 26 and 35 cm in Figures 5a and 5b, respectively. The regions that show the characteristics of the maritime regime include the North Cascades, the Cascades, the Klamath Mountains, and the Sierra Nevada Mountains (Figure S2).

On the other hand, when compared to the accumulation patterns in the maritime regions, the continental regions exhibit a pattern characterized by lower maximum accumulations below 200 cm and longer snow accumulation season lengths lasting as long as 260+ days, occupying the upper-left portion of the point-cloud (e.g., the Middle and Southern Rocky Mountains in Figures 5e and 5f, respectively). For these continental regions, the mean length of the accumulation season (inset boxes in Figures 5e and 5f) follows a steep linear increase with peak SWE for the shallower snowpacks ($\beta_1 = 7.0$ and 6.7 d/cm in Figures 5e and 5f, respectively), while a milder slope for the deeper snowpacks ($\beta_2 = 0.09$ and 0.27 d/cm in Figures 5e and 5f, respectively). The intersect of these regression lines is located at 23 and 22 cm in Figures 5e and 5f, respectively; however, the transition from the regression slopes for the shallower and deeper snowpacks is more asymptotic and gradual than the one observed in the maritime region. Regions showing this pattern include the Middle Rockies, the Wasatch and Uinta Mountains, and the Southern Rockies (Figure S3).

The intermountain regime lies in between these two patterns (e.g., the Blue Mountains and the Northern Basin and Range in Figures 5c and 5d, respectively). β_1 slopes are 4.9 and 6.1 d/cm in Figures 5c and 5d, respectively. β_2 slopes are 0.25 and 0.31 d/cm in Figures 5c and 5d, respectively. The intersect of these

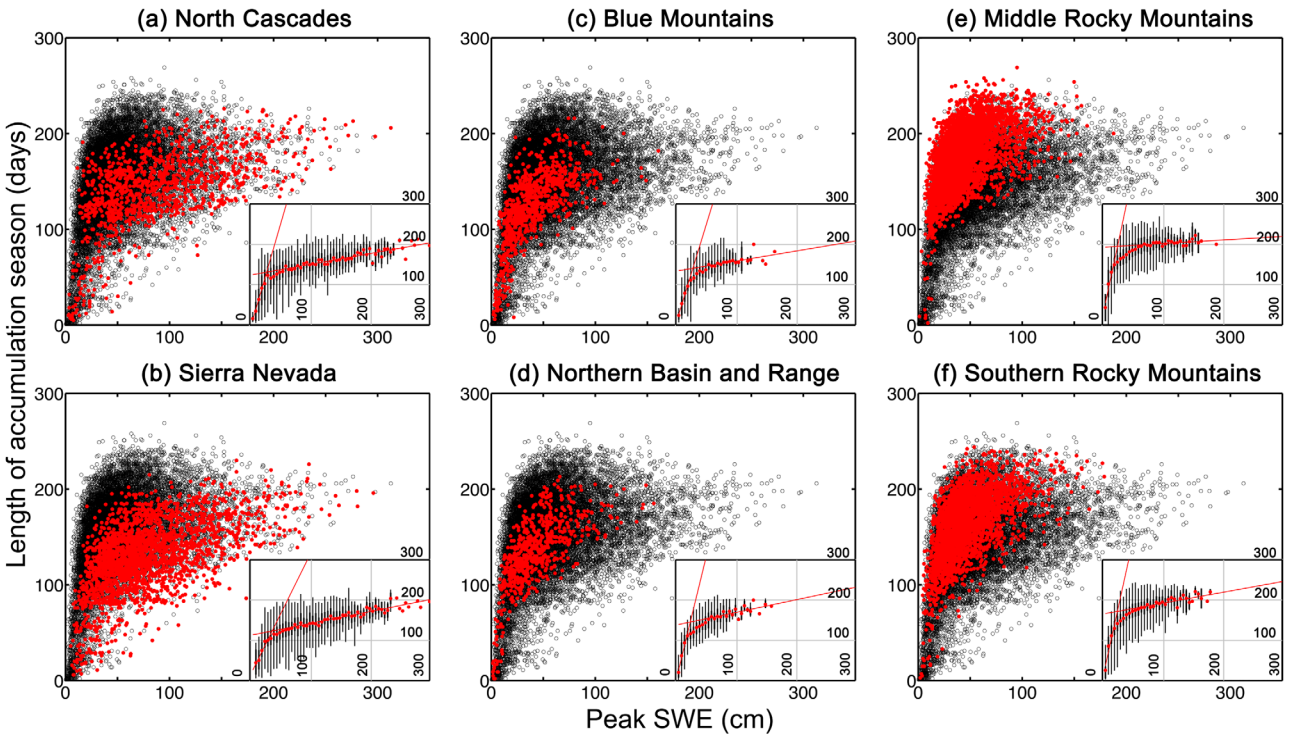

Figure 5. Scatter plots of the yearly pairs of the length of the snow accumulation season versus peak SWE for all of the snow pillow stations in the Western U.S. (black circles). Six ecoregions are highlighted (red circles): two of them representing the (a, b) maritime climate, two representing the (c, d) intermountain climate, and two representing (e, f) continental climates. The ecoregions are (a) North Cascade mountains, (b) the Sierra Nevada Mountains, (c) the Blue Mountains, (d) the Northern Basin and Range, (e) the Middle and (f) Southern Rocky Mountains. The plots display a total of 18,498 year-pairs (black circles), with 1118 year-pairs in the North Cascades, 2236 in the Sierra Nevada Mountains, 837 in the Blue Mountains, 675 in the Northern Basin and Range, 3777 in the Middle Rocky Mountains, and 2957 in the Southern Rocky Mountains. The boxplots in the lower-right quadrant of each plot correspond the red circles grouped in bins of 5 cm of peak SWE to better display the distribution of the values in the scatter plots. The black wider boxes mark the values within the 25% and 75% quantiles, and the whiskers (lines) mark the extent of all of the values within each bin.

regression lines is located at 26 and 22 cm in Figures 5c and 5d, respectively. Regions showing this pattern include the Eastern Cascades slopes and foothills, the Blue Mountains, Northern and Central basins and ranges, the Columbia Mountains/Northern Rockies, the Idaho Batholith, and the Canadian Rockies (Figure S4). The metrics from the stations in Arizona/New Mexico region do not show the characteristics of the regimes above because of the intermittent and shallow snowpacks of the region (Figure S5a). This shallow and intermittent snowpacks do not have a clear initial, peak, and meltout dates in the sense analyzed here because the snow cover results from individual or closely occurring snow storms whose timing, magnitude, and duration and meltout are strongly controlled by the meteorological conditions of the region during the winter and spring seasons.

3.4. Regional Differences in Ablation Dynamics

Similarly, we characterize the ablation period by analyzing the relationship between the ablation slope and the timing of peak SWE, which we treat as an indicator of the onset of the snowmelt season. Regional patterns also emerge when the different regions are highlighted. Maritime regions show earlier onsets of the snowmelt season and higher ablation slopes reaching values as high as 6 cm/d, occupying the upper-left portion of the point-cloud (e.g., the North Cascades and Sierra Nevada Mountains in Figures 6a and 6b, respectively). On the other hand, the continental regions exhibit later snowmelt season onsets and lower ablation slopes below 4 cm/d, occupying the lower-right portion of the point-cloud (e.g., the Middle and Southern Rocky Mountains in Figures 6e and 6f, respectively). Once again, the intermountain region is located between these two patterns (e.g., the Blue Mountains and the Northern Basin and Range in Figures 6c and 6d, respectively), and the metrics of the Arizona/New Mexico region do not show the characteristics of the regimes above because the intermittent and shallow snowpacks of the region lead to several accumulation and melt cycles that are difficult to characterize using the metrics studied here (Figure S5b).

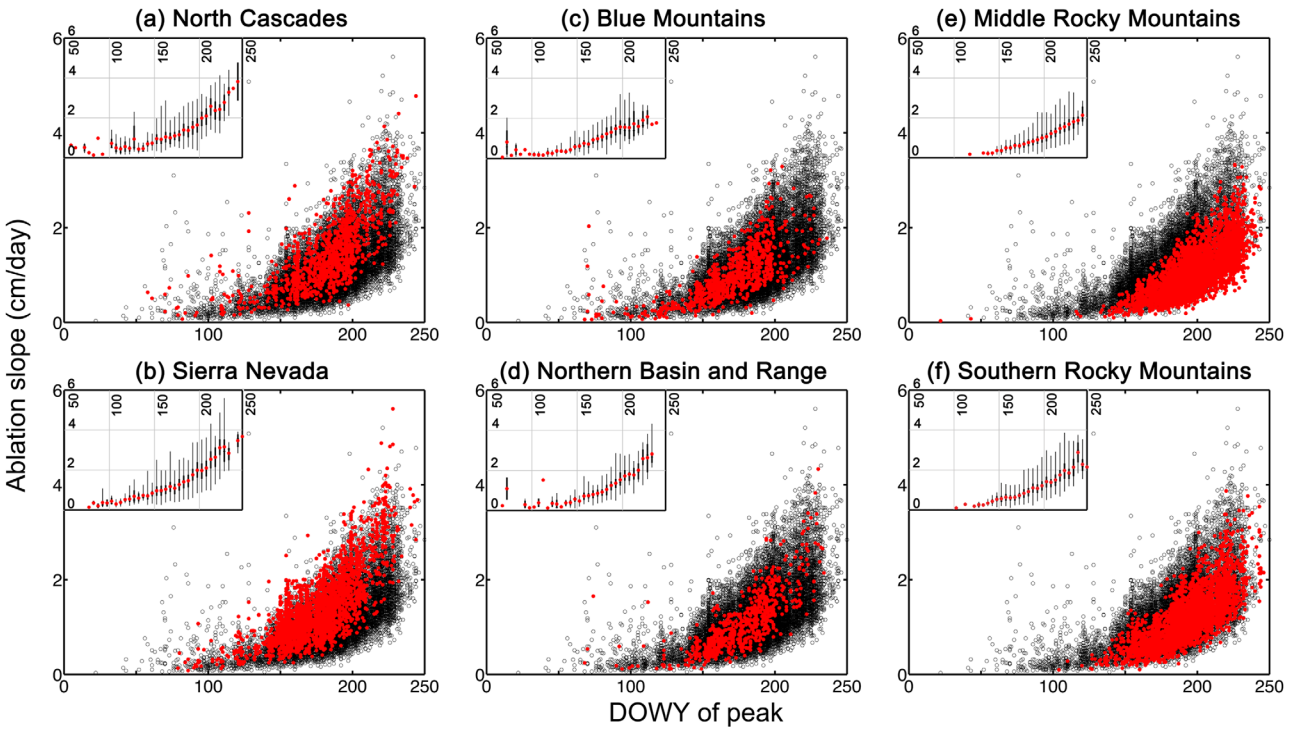

Figure 6. Scatter plots of the yearly pairs of the ablation slopes versus the day of water year of peak SWE (DOWY of peak) for all of the snow pillow stations in the Western U.S. (black circles). Six ecoregions are highlighted (red circles): two of them representing the (a, b) maritime climate, two representing the (c, d) intermountain climate, and two representing (e, f) continental climates. The ecoregions are (a) North Cascade mountains, (b) the Sierra Nevada Mountains, (c) the Blue Mountains, (d) the Northern Basin and Range, (e) the Middle and (f) Southern Rocky Mountains. The plots display a total of 18,659 year-pairs (black circles), with 1118 year-pairs in the North Cascades, 2362 in the Sierra Nevada Mountains, 836 in the Blue Mountains, 674 in the Northern Basin and Range, 3785 in the Middle Rocky Mountains, and 2964 in the Southern Rocky Mountains. The boxplots in the upper-left quadrant of each plot correspond the red circles grouped in bins of 5 days (*x* axis). The black wider boxes mark the values within the 25% and 75% quantiles, and the whiskers (lines) mark the extent of all of the values within each bin.

Figures S6, S7, and S8 show the highlighted point-clouds for all the ecoregions in the maritime, continental, and intermountain regimes, respectively, along with the respective locations across the Western U.S.

4. Discussion

Causal factors regarding the differences in snow accumulation and snowmelt metrics within the different regions are highly variable across the Western U.S. The gradients in snow accumulation dynamics from maritime to continental regions reflect winter precipitation patterns. Snow accumulation in maritime regions is dominated by land-reaching winter Atmospheric Rivers (AR's) events that deliver large amounts of snow over short periods of time (1–2 days), with moisture from the Pacific Ocean encountering the topographic barriers and undergoing orographic lifting [*Neiman et al*., 2008; *Guan et al*., 2010]. Winter atmospheric rivers have been shown to deliver 2–4 times as much SWE as normal non-AR storms in some areas of the Pacific Northwest [*Neiman et al*., 2008; *Guan et al*., 2010], and ARs contribute between 25% and 50% of total seasonal SWE in some regions [*Guan et al*., 2010]. These large snowfall events allow for deep snowpack accumulation over shorter periods as indicated in Figures 5a and 5b. On the other hand, winter and spring precipitation in the continental regions is dominated by frontal storms associated with temperatures significantly below freezing and low-precipitation (PRE) intensities [*Serreze et al*., 1999], leading to longer accumulation seasons (Figures 5e and 5f). Moreover, SWE/PRE ratios are higher in the continental regions allowing for greater snow accumulation for a given amount of precipitation [*Serreze et al*., 1999]. The intermountain region lies in between because of moderate temperatures and reduced atmospheric water vapor concentrations associated with increased distances from the Pacific Ocean moisture source (Figures 5c and 5d) [*Serreze et al*., 1999].

Ablation dynamics are also markedly different from maritime to continental environments. Gradients in temperature, seasonality, solar irradiance, cloud cover, and precipitation patterns during the spring season

are all primary controllers of the gradients illustrated in Figure 6. In particular, air temperatures during springtime precipitation events can dramatically alter snow season length. Warmer maritime regions and lower elevations exhibit decreased SWE/PRE ratios in spring leading to earlier melt. Conversely, colder, continental regions and higher elevations exhibit greater SWE/PRE ratios in spring leading to later melt. In this regard, the onset of above-freezing temperatures in maritime regions generally occurs between March and April versus April and May in continental regions, and with intermountain regions in between [*Serreze et al*., 1999]. The effects of these temperature gradients from maritime to continental regions can be exacerbated by seasonality in precipitation, whereby continental regions have relatively high incidence of spring precipitation [*Serreze et al*., 1999].

The relationships between melt rates and the timing of peak SWE are quite instructive of snowmelt processes. In this regard, years with later snowmelt occur at a time of year with higher solar elevations and therefore greater solar irradiance. The coupling of the greater atmospheric air temperatures with higher solar irradiance results in particularly high available energy at the snowpack atmosphere interface which drives the greater melt rates [*Jepsen et al*., 2012]. In warmer regions, rain-on-snow events, particularly toward the northern maritime regions, may also be important [*McCabe et al*., 2007]. It is important to note that detailed characterization of the mechanisms responsible for the gradients in the snow metrics is beyond the scope of this work.

In general, within each regime there is a clear trade-off between latitude and elevation. Southern versus northern regions show little differences in relationships between peak snow accumulation and snow accumulation season length (Figure 5). Pearson correlation coefficients between the mean series of the maritime and continental example regions in Figure 5 (red dots in inset plots) are 0.96 and 0.98, respectively. Similarly, latitudinal differences in relationships between ablation slope and DOWY of peak SWE are not apparent (Figure 6). Pearson correlation coefficients between the mean series of the maritime and continental sample regions in Figure 6 (red dots in inset plots) are 0.96 and 0.97, respectively. However, stations in the northern regions are located within lower elevation ranges with respect to those in the southern regions (Figure S9). For example, stations in the Northern Cascades are located between 515 and 1980 m, with mean elevation of 1290 m, while stations in the Sierra Nevada are between 1570 and 3475 m, with mean elevation of 2455 m. These trade-offs are also seen in the timing of initial snow accumulation with only 7 days difference on average between the Sierra Nevada and Northern Cascades (Figure S10). This trade-off is present in the three regimes (i.e., maritime, intermountain, continental) and helps to explain the relative consistency.

As regional warming continues, a shift toward earlier spring snowmelt is generally expected, especially at lower elevations where rainfall versus snowfall apportionments may be most sensitive to temperature increases [*Barnett et al*., 2005]. These changes would affect lengths of the accumulation and melting periods, and the snow cover duration. Similarly, snow accumulations may be significantly affected, which, depending on the direction of these effects, the changes in maximum accumulation may lead toward shorter accumulation and melt periods and faster melt rates. The metrics analyzed here provide a basis for establishing baseline system behavior whereby future changes in snowpack processes could be compared to.

The regional variations in the relationships described above can be used in a statistical framework to determine what type of regime exists at a particular measurement location according to the position of the year-pairs of some of the SWE metrics analyzed here (Figure 7). On this basis, a metric that indicates the likeliness that the year-pairs between two particular SWE metrics belong to a given regime can be defined based on the average probability density of the year-pairs when plotted in the pdf's in Figure 7. For the accumulation dynamics, the procedure can described as follows: the scatter points from a measurement location (e.g., a snow pillow station) for which there are N year-pairs of accumulation season length versus peak SWE can be plotted in Figure 7a to obtain N probability density values, one for each point (i.e., value of the probability density that the point lies on). From these values, an average probability density for the location can be obtained as

$$\overline{PD_{regime}} = \frac{1}{N}\sum_{i=1}^{N} PD_i \tag{1}$$

where $\overline{PD_{regime}}$ stands for the average probability density at a given location for a given regime (i.e., maritime, intercontinental, and continental, as there is one pdf per regime for the accumulation period), PD_i is the probability density for the ith point/year-pair obtained from the pdf's corresponding to each regime.

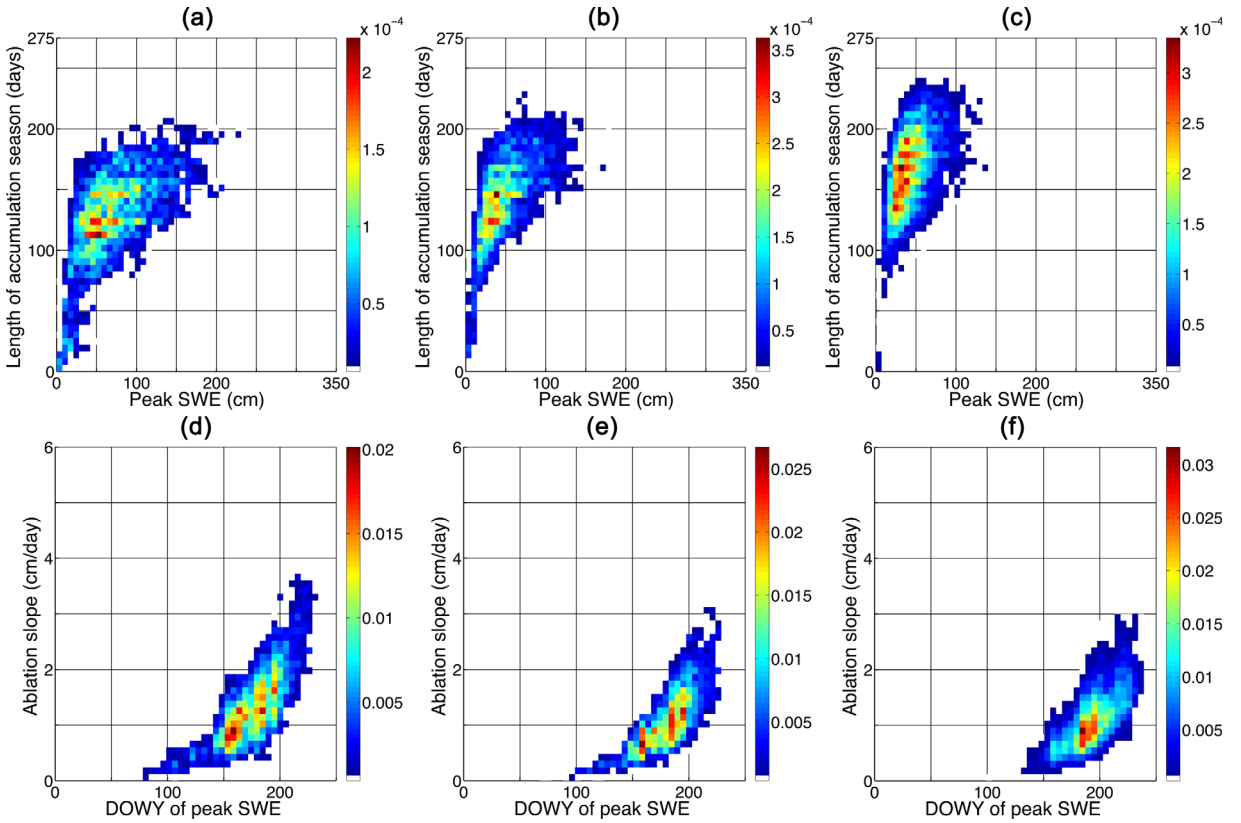

Figure 7. Empirical probability density functions (EPDF) derived for the relationships between the length of the snow accumulation season versus peak SWE, and ablation slope versus DOWY of peak SWE. The EPDF's on the left plots (Figures 7a and 7d) are derived from the year-pairs of the stations in the maritime regions, the middle panels (Figures 7b and 7e) are derived from the stations in the intermountain regions, and the right panels (Figures 7c and 7f) are derived from the stations in the continental regions. The volume under the surfaces equal one, and the distribution can be used to determine whether a series of year-pairs belong to a particular snow regime.

A location with an accumulation pattern similar to that observed in the maritime regime will have a higher average probability density from Figure 7a ($\overline{PD_{maritime}}$) than the same average probability density derived using Figures 7b and 7c ($\overline{PD_{intermountain}}$ and $\overline{PD_{continental}}$, respectively). Following this procedure, we can use the pdf's for the maritime, intermountain, and continental regimes to determine an average probability density using (1). These three average probability densities (one derived from each $\overline{PD_{maritime}}$, $\overline{PD_{intermountain}}$, and $\overline{PD_{continental}}$) can be compared with each other to estimate the likelihood that the accumulation patterns at a particular location is closer to any of the three regimes. The same procedure can be performed for the ablation period using the pdf's based on the ablation period metrics (e.g., Figures 7d–7f). On this basis, a rescaled metric (M_{regime}) of this likelihood is defined as

$$M_{maritime} = \frac{\overline{PD_{maritime}}}{\frac{1}{3}\left(\overline{PD_{maritime}} + \overline{PD_{intermountain}} + \overline{PD_{continental}}\right)} \tag{2.1}$$

$$M_{intermountain} = \frac{\overline{PD_{intermountain}}}{\frac{1}{3}\left(\overline{PD_{maritime}} + \overline{PD_{intermountain}} + \overline{PD_{continental}}\right)} \tag{2.2}$$

$$M_{continental} = \frac{\overline{PD_{continental}}}{\frac{1}{3}\left(\overline{PD_{maritime}} + \overline{PD_{intermountain}} + \overline{PD_{continental}}\right)} \tag{2.3}$$

If the accumulation pattern (or ablation pattern) is closer to that of the maritime regime, then $M_{maritime}$ will be larger than $M_{intermountain}$ and $M_{continental}$. Similarly, if the accumulation pattern (or ablation pattern) is closer to that of the continental regime, then $M_{continental}$ will be larger than $M_{maritime}$ and $M_{intermountain}$. This procedure is repeated for all stations. The rescaled metric values can then used to map the type of regime that the measurement locations exhibit across the Western U.S.

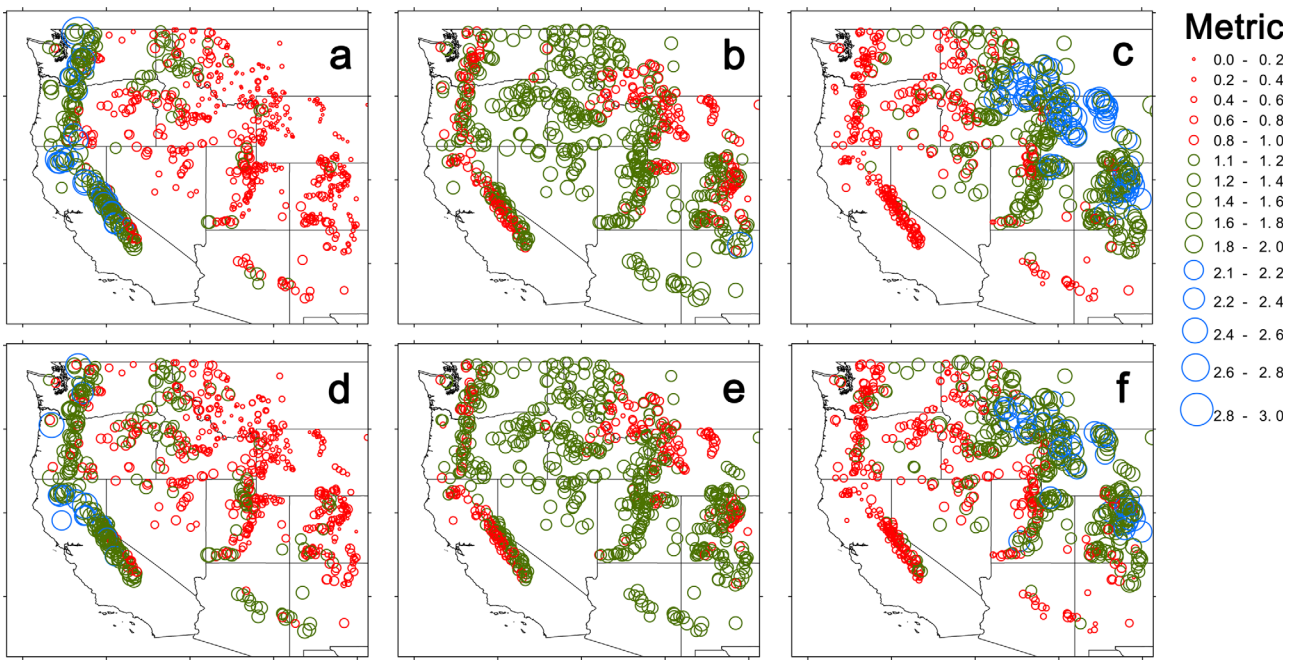

Figure 8. Rescaled metric, M_{regime}, that a station shows the characteristics of the maritime, intermountain, or continental regime. The top plots (a, b, c) correspond to the accumulation period and present the rescaled metrics $M_{maritime}$, $M_{intermountain}$, and $M_{continental}$, respectively. Similarly, the bottom plots (d, e, f) correspond to the ablation period and present the rescaled metrics $M_{maritime}$, $M_{intermountain}$, and $M_{continental}$, respectively.

The procedure leads to six maps showing the spatial variation of the rescaled metrics across the Western U.S. (Figure 8). The rescaled metrics highlight the differences in the accumulation and ablation periods across the Western U.S. The metric values obtained using the maritime regime pdf's (Figures 8a and 8d) decrease rapidly toward the East, with the highest values closest to the Pacific Ocean, and lowest values toward the easternmost portion of the mountain ranges of the continental U.S. Similarly, the highest values for the rescaled metric from the intermountain pdf's highlight that the stations displaying these relationships are located along the intermediate portions of the Western U.S., decreasing toward both the east and the west (Figures 8b and 8e). Lastly, the rescaled metric from the continental pdf's consistently show that the stations with the highest metric values are located toward the easternmost portions of the mountain ranges in the Western U.S., decreasing toward the West with the lowest values closest to the Pacific Ocean.

The maps in Figure 8 highlight the natural variability of the SWE curve across the regions during the accumulation and ablation seasons. Clearly, there is a strong climatic signal that is reflected in the statistical properties of the SWE curve across the continental US. The metrics analyzed could be used to identify whether a station exhibits a regime that is closer to the three regimes identified in this analysis from a purely statistical perspective. Moreover, these metrics can be used to identify changes in station behavior—for example, a lower elevation station in the continental region may begin to map more closely to the intermountain regime due to increases in temperature. The regime classification shown herein provides an important linkage between broad hydrologic signals (e.g., the timing and magnitude of snow accumulation and snowmelt) and variability in climate and the physical environment (e.g., elevation, orography, latitude, and continentality)—an important aspect of hydrologic classifications [*Wagener et al*., 2007]. Furthermore, *Wagener et al*. [2007] argue that hydrologic classifications should either account for changes in climate or should elucidate hydrologic response to changes in climate and associated drivers of change. While the work presented here does not explicitly identify the drivers of the regime classification, the use of both snow accumulation and snowmelt metrics as the basis for the classification focuses the analysis on the most germane hydrologic response with respect to climate change. In this context, changes in rain versus snowfall proportions and the timing and magnitude of snowmelt are considered to be primary drivers of hydrologic response to climate change [*Barnett et al*., 2005].

Analyses of the impacts of climate change in the mountain ranges of the Western U.S. have shown statistically significant increasing trends in temperature and precipitation in the twentieth century [*McCabe and*

Wolock, 2002; *Mote*, 2003a, 2003b], downward trends in spring SWE accumulations [*Hamlet et al*., 2005], earlier snow melt and peak spring streamflow timing [*Stewart et al*., 2005], and increases in rainfall versus snowfall apportionments [*Knowles et al*., 2006]. Model projections of snowmelt timing indicate future shifts toward earlier melt and snow disappearance, with greatest sensitivities in areas where air temperatures hover around 0°C [*Knowles and Cayan*, 2004; *Nolin and Daly*, 2006]. Also, a decrease in snow cover duration is expected with regional warming, which has significant implications for the surface energy balance given the drastic differences in albedo between snow-covered versus snow-free landscapes. Also, recent studies have observed increased frequency and intensity of dust-on-snow events which have advanced the timing of snowmelt by weeks relative to dust-free conditions [*Painter et al*., 2010]. These various perturbations to the proportions of the SWE curve may lead to the crossing of thresholds in which system behavior is indefinitely altered. Our methodology provides a basis for baseline snow regime classification whereby future changes in SWE curve proportions can be evaluated.

5. Conclusions

Persistent proportions of the SWE curve emerge from this analysis. The length of the snow accumulation season and total snow season length increases with peak SWE for values below 40 cm. Later snow disappearance dates correspond with deeper snowpacks and later peak SWE timing correspond with significantly faster snowmelt. Three snowpack regimes emerge from the analyses of the accumulation and melting proportions of the SWE curve, corresponding with climatic regimes of the Western U.S.: a maritime, an intermountain, and a continental regime. The maritime regime exhibits the largest peak snow accumulations, the shortest accumulation season lengths, earlier snowmelt season onsets, and higher ablation slopes. The continental regime exhibits lower peak snow accumulations, longer accumulation season lengths, later snowmelt season onsets and lower ablation slopes. The intermountain regime lies between these two accumulation and snowmelt patterns. Statistical analysis of intraregional variability in station behavior, relative to regional average behavior, highlights the natural variability of the SWE curve within regions and provides a framework to identify changes in station behavior, e.g., in response to changes in climate. The metrics introduced also provide a basis for establishing baseline SWE curve proportions to which future changes in snowpack processes could be compared. Increases in temperatures and precipitation, downward trends in spring SWE accumulations, earlier snowmelt, and increases in rainfall versus snowfall apportionments, among other changes, will affect the relationships presented herein, and their effects in snowpack dynamics across the Western U.S. could be identified through the use of simple metrics such as the ones introduced here.

Acknowledgments
This research was supported by NASA grant NNX11AK35A, NSF grants EAR 1032295, EAR 1141764, and EAR 1331828, USDA grant 2012–67003-19802, and the NOAA RISA Western Water Assessment. Part of NPM's contributions to this study was carried out on behalf of the Jet Propulsion Laboratory, California Institute of Technology, under a contract with the National Aeronautics and Space Administration.

References

Barnett, T. P., J. C. Adam, and D. P. Lettenmaier (2005), Potential impacts of a warming climate on water availability in snow-dominated regions, *Nature*, *438*(7066), 303–309.

Commission for Environmental Cooperation (2009), *Ecological regions of North America, Level 3, scale 1:4,000,000*, Commission for Environmental Cooperation, Montreal, Quebec, Canada.

Flanner, M. G., K. M. Shell, M. Barlage, D. K. Perovich, and M. A. Tschudi (2011), Radiative forcing and albedo feedback from the Northern Hemisphere cryosphere between 1979 and 2008, *Nat. Geosci.*, *4*(3), 151–155.

Gray, D. M., and D. H. Male (Eds.) (1981), *Handbook of Snow: Principles, Processes, Management and Use*, 776 pp., Pergamon, Toronto, Ont., Canada.

Guan, B., N. P. Molotch, D. E. Waliser, E. J. Fetzer, and P. J. Neiman (2010), Extreme snowfall events linked to atmospheric rivers and surface air temperature via satellite measurements, *Geophys. Res. Lett.*, *37*, L20401, doi:10.1029/2010GL044696.

Hall, A., and X. Qu (2006), Using the current seasonal cycle to constrain snow albedo feedback in future climate change, *Geophys. Res. Lett.*, *33*, L03502, doi:10.1029/2005GL025127.

Hamlet, A. F., P. W. Mote, M. P. Clark, and D. P. Lettenmaier (2005), Effects of temperature and precipitation variability on snowpack trends in the western United States, *J. Clim.*, *18*(21), 4545–4561.

Harpold, A. A., J. A. Biederman, K. Condon, M. Merino, Y. Korgaonkar, T. Nan, L. L. Sloat, M. Ross, and P. D. Brooks (2013), Changes in snow accumulation and ablation following the Las Conchas Forest Fire, New Mexico, USA, *Ecohydrology*, *7*, 440–452.

Jepsen, S. M., N. P. Molotch, M. W. Williams, K. E. Rittger, and J. O. Sickman (2012), Interannual variability of snowmelt in the Sierra Nevada and Rocky Mountains, United States: Examples from two alpine watersheds, *Water Resour. Res.*, *48*, W02529, doi:10.1029/2011WR011006.

Knowles, N., and D. R. Cayan (2004), Elevational dependence of projected hydrologic changes in the San Francisco Estuary and watershed, *Clim. Change*, *62*(1–3), 319–336.

Knowles, N., M. D. Dettinger, and D. R. Cayan (2006), Trends in snowfall versus rainfall in the Western United States, *J. Clim.*, *19*(18), 4545–4559.

Marks, D., and A. Winstral (2001), Comparison of snow deposition, the snow cover energy balance, and snowmelt at two sites in a semiarid mountain basin, *J. Hydrometeorol.*, *2*(3), 213–227.

McCabe, G. J., and M. D. Dettinger (1999), Decadal variations in the strength of ENSO teleconnections with precipitation in the western United States, *Int. J. Climatol.*, *19*(13), 1399–1410.
McCabe, G. J., and D. M. Wolock (2002), Trends and temperature sensitivity of moisture conditions in the conterminous United States, *Clim. Res.*, *20*(1), 19–29.
McCabe, G. J., M. P. Clark, and L. E. Hay (2007), Rain-on-snow events in the western United States, *Bull. Am. Meteorol. Soc.*, *88*(3), 319–328, doi:10.1175/Bams-88-3-319.
Molotch, N. P., and R. C. Bales (2005), Scaling snow observations from the point to the grid element: Implications for observation network design, *Water Resour. Res.*, *41*, W11421, doi:10.1029/2005WR004229.
Molotch, N. P., P. D. Brooks, S. P. Burns, M. Litvak, R. K. Monson, J. R. McConnell, and K. Musselman (2009), Ecohydrological controls on snowmelt partitioning in mixed-conifer sub-alpine forests, *Ecohydrology*, *2*(2), 129–142, doi:10.1002/eco.48.
Mote, P. W. (2003a), Trends in temperature and precipitation in the Pacific northwest during the twentieth century, *Northwest Sci.*, *77*(4), 271–282.
Mote, P. W. (2003b), Trends in snow water equivalent in the Pacific Northwest and their climatic causes, *Geophys. Res. Lett.*, *30*(12), 1601, doi:10.1029/2003GL017258.
Neiman, P. J., F. M. Ralph, G. A. Wick, J. D. Lundquist, and M. D. Dettinger (2008), Meteorological characteristics and overland precipitation impacts of atmospheric rivers affecting the West Coast of North America based on eight years of SSM/I satellite observations, *J. Hydrometeorol.*, *9*(1), 22–47.
Nolin, A. W., and C. Daly (2006), Mapping ''at risk'' snow in the Pacific Northwest, *J. Hydrometeorol.*, *7*(5), 1164–1171.
Painter, T. H., J. S. Deems, J. Belnap, A. F. Hamlet, C. C. Landry, and B. Udall (2010), Response of Colorado River runoff to dust radiative forcing in snow, *Proc. Natl. Acad. Sci. U. S. A.*, *107*(40), 17,125–17,130.
Pugh, E., and E. Gordon (2012), A conceptual model of water yield effects from beetle-induced tree death in snow-dominated lodgepole pine forests, *Hydrol. Processes*, *27*, 2048–2060, doi:10.1002/hyp.9312.
Rasmussen, R., et al. (2011), High-resolution coupled climate runoff simulations of seasonal snowfall over Colorado: A process study of current and warmer climate, *J. Clim.*, *24*(12), 3015–3048.
Rodríguez-Iturbe, I., G. Devoto, and J. B. Valdes (1979), Discharge response analysis and hydrologic similarity—Interrelation between the geomorphologic Iuh and the storm characteristics, *Water Resour. Res.*, *15*(6), 1435–1444.
Rutter, N., et al. (2009), Evaluation of forest snow processes models (SnowMIP2), *J. Geophys. Res.*, *114*, D06111, doi:10.1029/2008JD011063.
Serreze, M. C., M. P. Clark, R. L. Armstrong, D. A. McGinnis, and R. S. Pulwarty (1999), Characteristics of the western United States snowpack from snowpack telemetry (SNOTEL) data, *Water Resour. Res.*, *35*(7), 2145–2160.
Serreze, M. C., M. P. Clark, and A. Frei (2001), Characteristics of large snowfall events in the montane western United States as examined using snowpack telemetry (SNOTEL) data, *Water Resour. Res.*, *37*(3), 675–688.
Stewart, I. T., D. R. Cayan, and M. D. Dettinger (2005), Changes toward earlier streamflow timing across western North America, *J. Clim.*, *18*(8), 1136–1155.
Stocker, T. F., D. Qin, G.-K. Plattner, M. Tignor, S. K. Allen, J. Boschung, A. Nauels, Y. Xia, V. Bex, and P. M. Midgley (Eds.) (2013), *IPCC, 2013: Climate Change 2013: The Physical Science Basis. Contribution of Working Group I to the Fifth Assessment Report of the Intergovernmental Panel on Climate Change*, 1535 pp., Cambridge Univ. Press, Cambridge, U. K.
Sturm, M., J. Holmgren, and G. E. Liston (1995), A seasonal snow cover classification system for local to global applications, *J. Clim.*, *8*(5), 1261–1283.
Tague, C., and A. L. Dugger (2010), Ecohydrology and climate change in the mountains of the Western USA—A review of research and opportunities, *Geogr. Compass*, *4*(11), 1648–1663.
van Mantgem, P. J., et al. (2009), Widespread increase of tree mortality rates in the Western United States, *Science*, *323*(5913), 521–524, doi:10.1126/science.1165000.
Wagener, T., M. Sivapalan, P. Troch, and T. Woods (2007), Catchment classification and hydrologic similarity, *Geogr. Compass*, *1*(10.1111), 901–931.